




Instrumentation, cooling, and initial testing of a large, conduction-cooled, react-and-wind MgB_2 coil segment for MRI applications

D Zhang¹ , C Kovacs¹ , J Rochester¹, M Majoros¹ , F Wan¹, M D Sumption¹, E W Collings¹, M Rindfleisch², D Panik², D Doll², R Avonce², M Tomsic², C Poole³, L Sabri³, T Baig³ and M Martens³

¹ Center for Superconducting and Magnetic Materials (CSMM), MSE, The Ohio State University, Columbus, OH 43210, United States of America

² Hyper Tech Research Inc., Columbus, OH 43228, United States of America

³ Case Western Reserve University, Cleveland, OH 44106, United States of America

E-mail: zhang.5952@osu.edu

Received 30 March 2018, revised 1 June 2018

Accepted for publication 6 June 2018

Published 17 July 2018



Abstract

A react-and-wind MgB_2 coil segment for a conduction-cooled magnetic resonance imaging (MRI) machine has been fabricated and tested. The coil was developed as part of a collaborative effort on a conduction-cooled, MgB_2 -based, whole-body MRI image guided radiation therapy device. This study focuses on the fabrication, winding, instrumentation, cooling, and initial critical current (I_c) testing of this near-full-size MgB_2 segment coil. The coil was 0.9 m in diameter; the winding pack, 44.0 mm wide \times 50.6 mm high, used 1.7 km of an 18 filament MRI-style conductor with Nb chemical barriers, Cu interfilamentary matrices, and an outer monel sheath. The conductor was insulated and reacted before winding onto a stainless steel former. The coil was instrumented with Cernox and E-type thermocouple temperature sensors, strain sensors, and voltage taps. The conduction-cooled coil was mounted in a cryostat capable of accepting coils of up to 0.9 m in diameter and 0.5 m in height. Critical current measurements were performed as a function of temperature during a controlled heating of the coil. The operational target was $I = 200$ A at 13 K. The full magnet was designed to produce 0.75 T in the imaging area (at $I = 200$ A), with a maximum field of 1.93 T in the winding. The single segment coil measured here exceeded this operation specification, with an I_c of 280 A at 15 K and a maximum field 1.93 T in the winding. The coil was modeled using a finite element method, and a load line plot showed that 100% of short sample was reached at 21.5 K and above. These measurements demonstrate the viability of conduction-cooled MgB_2 background coils as replacements for liquid helium cooled NbTi background coils in future MRI devices.

Keywords: NbTi, MgB_2 , conduction cooling, magnetic resonance imaging, MRI, liquid helium, superconductor

(Some figures may appear in colour only in the online journal)

1. Introduction

Magnetic resonance imaging (MRI) has emerged as a popular noninvasive medical diagnostic tool. An important part of the MRI device is the magnet that produces the constant background field which polarizes the spins in a sample which is

being imaged. Nearly all medical MRI coils are wound with superconducting wire.

Two primary concerns for MRI manufacturers are cost and patient comfort. With regard to cost, we note that commercially available MRIs are generally equipped with NbTi coils operating at 4.2 K in liquid helium (LHe). However,

LHe is a non-renewable resource whose price has risen every year [1]. This has led to a demand for liquid cryogen free MRIs [2, 3]. Liquid cryogen free designs using NbTi conductors require significant cryogenic redesign, and demand much larger conductor operational margins. The fact that the minimum quench energy is relatively low for NbTi (less than 10 mJ) [4] leads to intrinsic design complications. On the other hand, medium temperature superconductors or high-temperature superconductors can be used in the conduction cooling mode without such limitations, since their minimum quench energies are one to two orders of magnitude higher than those of low temperature superconductors.

In order to increase patient comfort, one of the trends in industry has been towards shorter MRI machines. Open machines or more versatile machines are also of great interest. In addition to the potential cost advantages, conduction-cooled machines will allow much more flexibility in the design of the coils and their associated structures.

A recent paper which considers conductors beyond NbTi for MRI and the development of conduction-cooled MRI discusses various conductor options, including YBCO, Bi-based conductors, Nb₃Sn, and MgB₂ [5]. [5] concludes that while further development is required for all of these conductors, *in situ* MgB₂ is the conductor with the most potential to replace NbTi for 1.5 T MRI use.

Our group has studied *in situ* MgB₂ conductors for a number of years, and they have shown promise for MRI applications [6, 7]. Alternatively, Columbus superconductors was able to produce *ex situ* Cu-stabilized multifilamentary MgB₂ tapes [8] for use in applications including MRI. However, as discussed in [5], the performance of the Hyper Tech Research produced kilometer-long MgB₂ wires [9] has a performance more matched to the requirements of 1.5 T whole-body MRI magnets.

Beyond conductor development, a significant number of MgB₂ coils have been made since 2002. Early on, most of coils which were made had small dimensions. Our group has studied the properties of small helical coils [10], larger react-and-wind (R&W) and W&R coils [11] (winding OD of 108.9 and 31.8 mm height), and racetrack coils with ODs of 220–232 mm [12, 13]. Takahashi *et al* [14] reported an MgB₂ solenoid coil of dimension 60.0 mm (height) and 51.3 mm OD [14]. Park *et al* [15] demonstrated a coil (292 mm OD × 25 mm) operating in LHe and explored quench protection. More recently, Ye *et al* [16] tested two conduction-cooled MgB₂ coils, one of which was a single layer test coil and the other a pancake coil (each with 200 mm OD) exploring the stability and quench behavior. Wang *et al* [17] used IMD fabricated MgB₂ wire for making two solenoid coils; the winding pack dimensions for the larger coil were 57.8 mm OD by 60.0 mm high. An MgB₂ coil cooled by solid nitrogen (SN₂) was fabricated and measured by Patel *et al* [18]. The coil had an inner diameter of 109 mm and a height of 20 mm; the persistent mode was evaluated for the coil. At a much larger scale, a fully operational open MRI system with a gap nominal field of 0.5 T designed by Columbus superconductor [19] has been demonstrated. It had a winding OD of 2 m and a height of 2.4 m. This MRI system was fully functional although it did use an iron yolk. Our recent focus

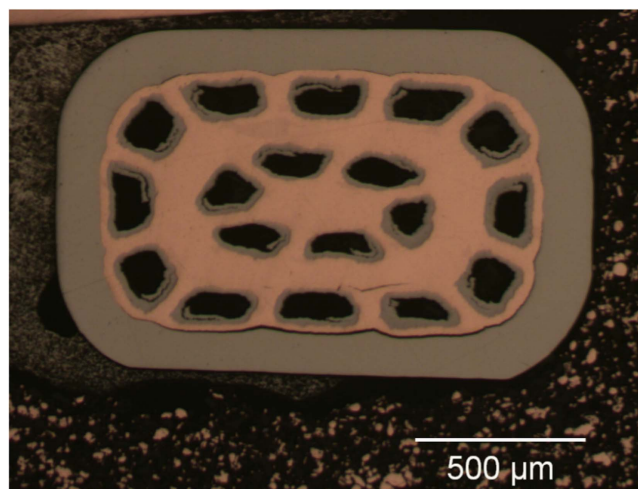


Figure 1. Architecture of MgB₂ conductor used, conductor is 1.5 mm wide × 1.0 mm thick.

has been the development of segment coils for whole-body MRI. We tested a sub-size MRI coil segment in 2016 [20] using conduction cooling. This present work is a follow-on, and is a nearly full-size MgB₂ segment coil (as designed for whole-body MRI applications). Our particular application for this coil is as part of an image guided therapy MRI design, which is an exciting application for MgB₂ magnets [21]. Image guided MRI systems differ from conventional 1.5 T MRI systems because in these systems an MRI is used to locate a tumor which is then irradiated (x-rays) while in the machine. This required that the main coils of the MRI (as well as the cryostat that cools them) be separated into two groupings to allow x-ray treatment access, which significantly increases magnet difficulty. Much larger magnets than for standard whole-body MRI are required to reach a given field. Additionally, an interaction of the secondary electrons generated by the x-ray beam and the MRI field adds additional system complications [21]. For both of these reasons, some image guided therapy MRI designs use fields lower than 1.5 T, e.g. the 0.75 T (for the whole eight-magnet MRI, at the field center) of our present design.

In this work we report on the use of a R&W method for manufacturing a conduction-cooled MgB₂ coil segment. The use of a R&W approach rather than wind-and-react approach avoids the need for the use of high-temperature compatible insulation and facilitates the fabrication of large coils. Below we first describe the conductor used, followed by the segment coil winding and instrumentation, followed by cryogenic tests of the coil segment. Finally we demonstrate that the coil more than meets the design current of 200 A at 13 K (1.93 T on winding), and that the load line met short sample at 21.5 K and above.

2. Experimental details

2.1. Conductor specifics

The conductor used was an MRI-specific MgB₂ strand manufactured by Hyper Tech Research Inc. (HTR) using an *in situ*

Table 1. Specifications of the MgB₂ conductor (Strand #3700).

Filament number	Chemical barrier	Interfilamentary matrix	Outer sheath	Central fil (s)	Dopant	Total area (mm ²)	% powder
18	Nb	Cu	Monel	Cu	C	1.47	12.5

Table 2. Specifications for MgB₂ segment coil.

Former material	Winding pack OD	Winding pack ID	Winding height	No. of turns	No. of layers	Turns per layer	Total conductor length
304 SS	901.3 mm	867.3 mm	50.6 mm	636.5	22	29	1744.4 m

**Figure 2.** Current lug with voltage taps V37 and V38.

CTFF powder-in-tube process. The strand, shown in figure 1, was 1.5 mm wide by 1.0 mm thick, and had a Cu interfilamentary matrix, Nb chemical barriers, and a Monel outer sheath. The conductor is described in table 1 and has the exact specifications of the conductor as detailed in [22]. The Mg: B powder ratio was 1:2 and used standard Mg powder (99%, ~325 mesh) and very fine (50–100 nm) size pre-carbon-doped boron as described in [23]. The wire was first insulated and then wound onto a 304 stainless steel former and heat treated at 675 °C for 60 min in a retort under an Ar atmosphere. It was then wound onto the final coil-former.

2.2. Coil winding

Table 2 shows the specifications of the segment coil. The final former which the insulated and pre-reacted MgB₂ wire was wound onto was a 304 stainless steel/Cu composite coil-former with an ID of 857 mm and an OD of 901 mm. Care was taken during all handling operations to ensure that the strain limit of 0.2% was not exceeded. The coil-former itself was insulated prior to winding, in addition to the S-glass insulation present on the wire. As part of the winding process, the ends of the wire were soldered to current lugs as shown in figure 2, and certain voltage taps were installed in regions which would be inaccessible later in the coil fabrication process (the center tap, and two voltage taps, V38 and V40, described below). The coil winding was 44.0 mm wide by 50.6 mm

high, and had 22 layers, with 29 turns per layer. The coil required 1.74 km of 1.5 mm × 1.0 mm wire.

2.3. Instrumentation

After winding and before epoxy impregnation, the coil was instrumented with voltage taps, E-type thermocouples and Cernox temperature sensors (figure 3). After this, the coil was wrapped with E-glass insulation and vacuum epoxy impregnated. Subsequently, strain gauges and Cernox temperature sensors were applied.

Figure 3 shows the locations of the temperature sensors and strain gauges, and table 3 provides details of the temperature sensors and strain gauges. Five voltage taps were placed on the coil, one of which was located at the center of the coil winding (mid-length of the wire). Two voltage taps (V37 and V39) were located on the current injection lugs. Two additional voltage taps (V40 and V38) were placed two cm inboard of the current injection lugs to avoid the transfer voltage associated with current transfer into and out of the coil as depicted in figure 2. The instrumentation voltages, strain sensors, and Cernox sensor were connected by instrumentation wires to Fischer and Amphenol cryostat feed-throughs, which were wired to the external data acquisition (DAQ) system. The thermocouple wires were brought out to a second Amphenol connector and also brought to the DAQ system.

The coil was placed on a conduction-cooled Cu cold ring at the bottom of the cryostat (vacuum vessel). The cryostat, which can accommodate coils of up to 0.9 m in diameter and 0.5 m in height, used two Sumitomo CSW-71 compressors and RS415 cryocoolers to cool this ring. Cu cooling straps ran from the cold ring to the coil, and were bolted to it every 14.5 cm. In total, there were 20 sets of cooling straps connected to the coil in order to thermally sink it to the cryo-cooled Cu ring. Among these 20 sets, two sets were directly mounted to the Cu current injection lugs, and 18 sets were mounted onto the coil itself. Each Cu cooling strap was made up of eight 0.3 mm by 20 mm Cu strips, all coated with Apiezon N grease on the surface of each thin Cu lamination in the region of bolted contact, and secured using bolts torqued to 40 N m.

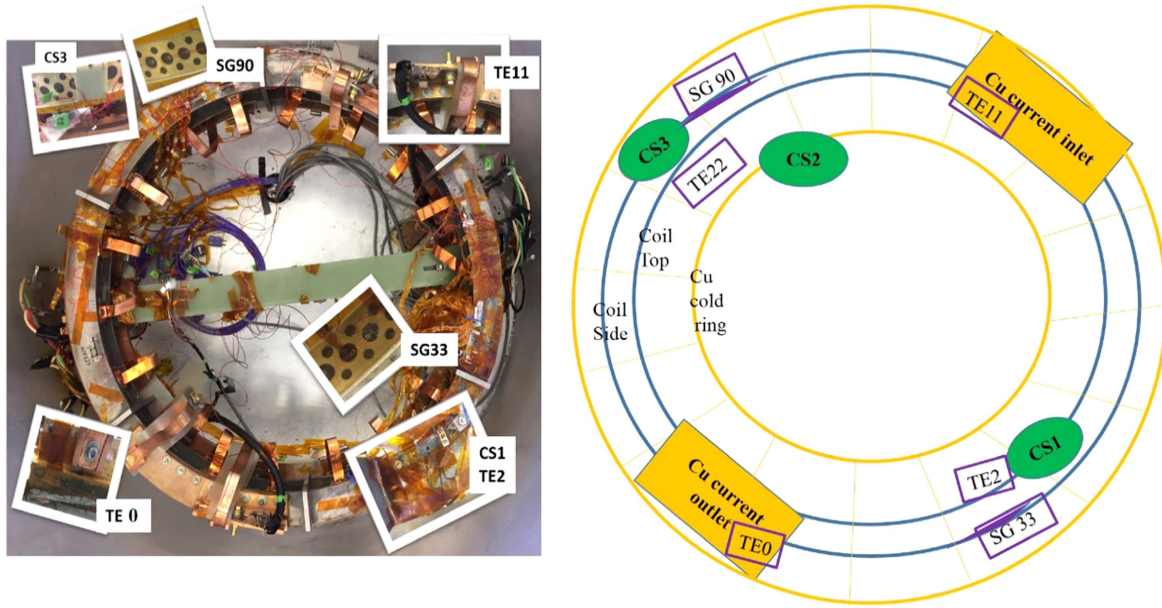


Figure 3. Top view of strain gauges and temperature sensors as placed on the coil; (left) annotated photograph, (right) schematic of temperature sensor and strain gauges layout ('TE' means thermocouple, 'CS' means Cernox sensor, 'SG' means strain gauge), showing current inlets and outlets in orange.

Table 3. Type and location of temperature sensor and strain gauges.

Name	Details	Location
Pt1	Platinum temperature sensor	On the first stage, left
Pt2	Platinum temperature sensor	On the first stage, right
CS1	Cernox temperature sensor	On top of the coil
CS2	Cernox temperature sensor	On Cu cold ring
CS3	Cernox sensor, with epoxy in between	On side of the coil
TE0	Type E thermocouple	On the Cu current outlet
TE2	Type E thermocouple	On top of the coil
TE11	Type E thermocouple	On the Cu current inlet
TE22	Type E thermocouple	Instrumentation zone
SG33	Strain gauge-axial direction	On side of the coil, near CS1
SG90	Strain gauge-axial direction	About 1.4 m away from SG33

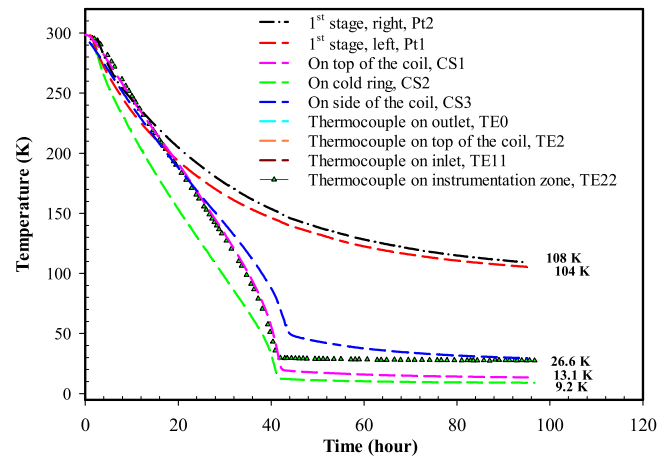


Figure 4. Temperature as a function of time at different locations during cool-down measurement.

3. Results and discussion

3.1. Cool-down measurements

After mounting the coil on the ring and putting the cryostat under vacuum, cool-down was initiated. During cool-down, a small current of 0.1 A was applied to the coil, and the voltage was monitored to measure the superconducting transition temperature (T_c). In addition, the coil temperature was measured by various sensors, and the reading of several strain sensors were monitored during cool-down.

Figure 4 shows the temperature and strain gauge readings as a function of temperature during cool-down. Because this was a relatively large coil, it took about 40 h to reach the base temperature of 9.3 K on the cold ring and 13.1 K on the top of the coil as measured by the Cernox sensors. As expected, a T_c

of 37 K (figure 4) was seen, consistent with the fact that C-doped MgB_2 samples are known to have a T_c slightly lower than 39 K of the undoped material [24]. The overlap of several temperature curves for sensors placed around the coil demonstrates the uniform cool-down of the coil.

The wire in the coil has several electrically conductive components: an outer sheath of Monel 400 (39%, cross-area fraction), a Nb chemical barrier (24%), a Cu interfilamentary matrix (27%) and MgB_2 filaments (10%). Using room temperature values of $\rho_{\text{Monel}} = 4.82 \times 10^{-5} \Omega \text{ cm}$ [25], $\rho_{\text{Cu}} = 1.72 \times 10^{-6} \Omega \text{ cm}$ [26], $\rho_{\text{Nb}} = 1.48 \times 10^{-5} \Omega \text{ cm}$ [27], and $\rho_{\text{MgB}_2} = 5.46 \times 10^{-4} \Omega \text{ cm}$ [28], the value for the conductor resistivity can be estimated. Since these components are in parallel the resistivity ($\rho_{\text{mix}} = \frac{1}{\sigma}$) of the mixture

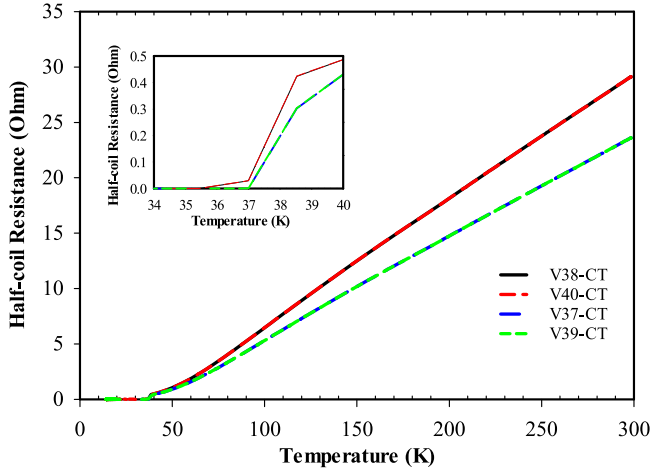


Figure 5. Coil resistance as a function of temperature during cool-down. Four measurements are shown, two from current injection to the center tap, and two from center tap to current extraction (using the two different sets of voltage taps near the current injection lugs). The sum of the two resistances is the whole coil resistance, and the difference in the two sets represents the fact that the center tap is not exactly at the center of length of wire used to wind the coil because the tap had to be made at the end of a winding layer.

given by:

$$\frac{1}{\rho_{\text{mix}}} = 0.39 \frac{1}{\rho_{\text{Monel}}} + 0.24 \frac{1}{\rho_{\text{Niobium}}} + 0.27 \frac{1}{\rho_{\text{Cu}}} + 0.1 \frac{1}{\rho_{\text{MgB}_2}} \quad (1)$$

is $5.6 \times 10^{-6} \Omega \text{ cm}$. Given the total length of the conductor and its cross sectional area, the resistance at room temperature is estimated to be 54Ω . This result compares well to the value of 55Ω measured at room temperature. Because the resistivity of Cu is more than one order of magnitude smaller (even at room temperature) than all of the other parallel components, the resistivity of the mixture is determined primarily by the area fraction and the resistivity of the Cu present in the cross section. The temperature dependence of electrical resistance is shown in figure 5.

3.2. Critical current (I_c) measurement

After the coil temperature stabilized at around 13 K, a series of critical current I_c measurements were carried out at temperatures ranging from 13.1 K–26 K. The temperature of the coil during each I_c run was measured (CS1) and is given in table 4, both at the start of the measurement, and at the finish. The first run (at 13 K) was performed at currents of up to 210 A. After this, the temperature was increased to 30 K, and I_c was measured at several temperatures as given in table 4 and figure 6 (right). To determine the critical current density J_c , an electric field criterion of 0.1 V cm^{-1} was used.

In addition to I_c , we wished to confirm a true zero resistance of the coil below I_c . Because the coil has an inductance, the voltage of the I – V curve has both a resistive and inductive component. The test coil's inductance is calculated by summing up the mutual inductance between two

Table 4. Temperature on top of the coil during I_c measurement.

Temperature of operation (K)	Temperature on top of the coil (K)	I_c (A)
13.1	Start: 13.07 End: 13.60	>211
15.9	Start: 15.90 End: 19.10	280
20.2	Start: 20.20 End: 24.80	>180
21.5	Start: 21.51 End: 22.50	261.6
24.8	Start: 24.79 End: 30.10	>203

currents loops on the same axis. The mutual inductance M between two current loops with radii a_1 and a_2 and axial positions z_1 and z_2 is [29]:

$$M(a_1, z_1, a_2, z_2) = 2\mu_0 \frac{\sqrt{a_1 a_2}}{k} \left(\left(1 - \frac{k^2}{2} \right) \times K(k) - E(k) \right), \quad (2)$$

where k is a function of a_1 , a_2 , z_1 and z_2 is defined as:

$$k = 2 \sqrt{\frac{a_1 a_2}{(z_1 - z_2)^2 + (a_1 + a_2)^2}}. \quad (3)$$

The term μ_0 is the permeability of free space ($4\pi \times 10^{-7} \text{ H m}^{-1}$), and $K(k)$ and $E(k)$ are the complete elliptic integrals of the first and second kind, respectively. The total inductance of the test coil then becomes the sum of equation (2) over the total number of layers N_r and the total number of loops-per-layer N_z of the test coil:

$$L = \sum_i^{N_r} \sum_j^{N_r} \sum_k^{N_z} \sum_l^{N_z} M(a_i, z_j, a_k, z_l). \quad (4)$$

When both $a_i = a_k$ and $z_j = z_l$, equation (2) does not apply, and the self-inductance of the single current loop must be calculated. Here, the self-inductance for each current loop is ignored when calculating equation (4). Using the equation (4), the calculated inductance for the test coil is 0.744 H .

The inductive voltage was calculated from the ramp rate and the inductance, and this voltage was removed from the I – V curve. The resulting I – V curve is shown in figure 6 (left) at 15.9 K. The slope is zero to within our measurement limit of $\pm 1 \times 10^{-8} \Omega$. Based on a coil length of 1.7 km, this amounts to a resistivity of $0 \pm 10^{-13} \Omega \text{ cm}$.

Shown in figure 6 (right) is the I_c value as a function of temperature. At 15.9 K, I_c was 280 A, significantly above our operational design of >200 A at 13.1 K.

Our design operating point was chosen to include certain safety factors. Bearing in mind the proper functioning of a full image guided magnet design (with all coil segments in place), the coil performance can be gauged in terms of the relationship of the load line to the short sample performance. In order to see if the load line reaches the short sample limit, we must first plot I_c versus the magnetic field B at various temperatures

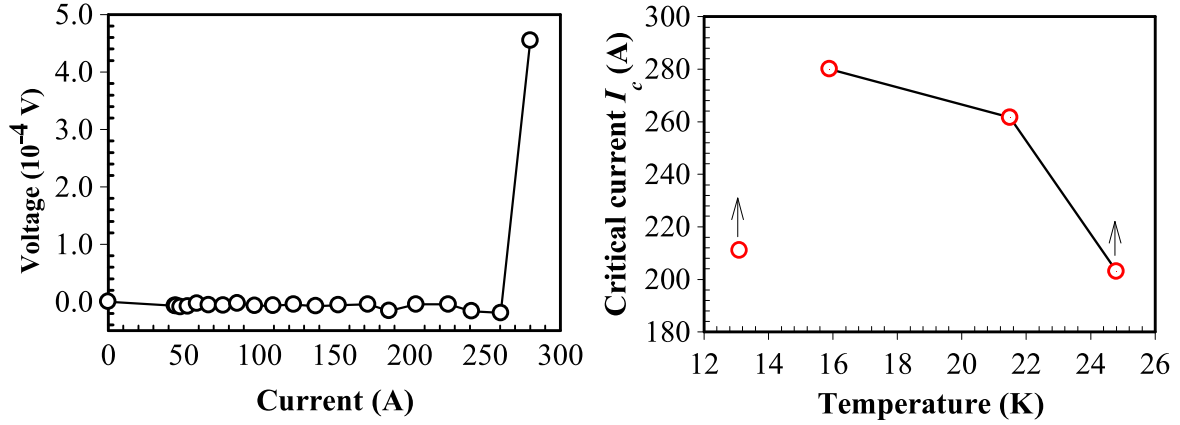


Figure 6. Representative I - V curve measured at 15.9 K (left) and I_c as a function of temperature (right).

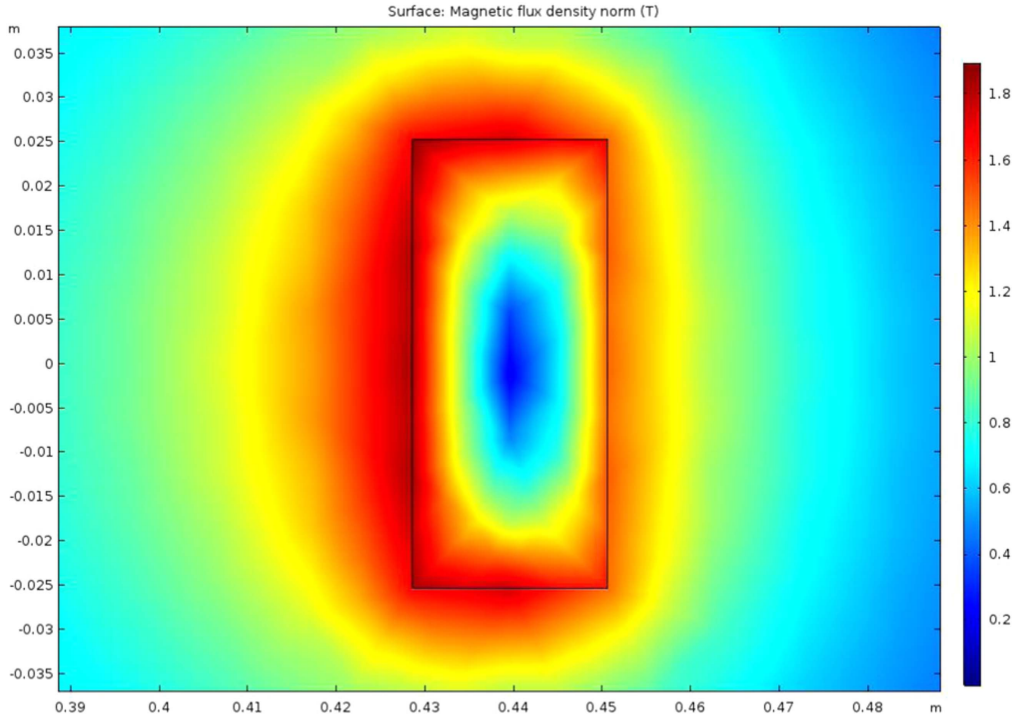


Figure 7. FEM model of the coil in 2D ($I = 280$ A/turn, number of turns = 636.5, $J_e = 1.60 \times 10^8$ A m $^{-2}$ winding).

for the conductor used for this coil. To do so, we can use the I_c - B curve which was measured at 4.2 K for the wire in question along with a fitting procedure developed by [30]. Here J_c for MgB $_2$ strands was seen to be well described by an exponential form

$$J_c(B, t) = J_{c0}(t) \exp(B/B_0(t)), \quad (5)$$

where J_{c0} is the zero-field temperature-dependent J_c , $t = T/T_c$ and $B_0(t)$ is a temperature-dependent field-normalization quotient. In order to solve $J_c(B, t)$ at different temperatures, two additional equations are needed [30], namely

$$J_{c0}(t) = J_{c00}(1 - \alpha t^2), \quad (6a)$$

$$B_0(t) = B_{00}(1 - \beta t), \quad (6b)$$

where J_{c00} represents (0 T, 0 K) critical current density and B_{00} is the 0 K value of B_0 . The parameters α and β describe the

quadratic temperature dependence of J_{c0} and the linear dependence of B_0 respectively. The use of $\alpha = 1.3$ and $\beta = 1.0$ were seen to work well both for binary and C-doped MgB $_2$ as well as the proper value of T_c was used [30]. Thus we use $\alpha = 1.3$ and $\beta = 1.0$, in conjunction with our measured T_c for this coil of 37 K and fitted equation (6) to our 4 K measurements of an short segment of the conductor (1 meter wound onto an ITER barrel) to give a parameterization of the wire, used below.

3.3. Finite element method (FEM) model of coil segment performance

The FEM model of the coil segment calculated by COMSOL Multiphysics is shown in figure 7. The red portion of the cross section represents the highest field region. We note in particular that the inner wall of the winding of the coil at the midplane of the coil represents the region with the highest

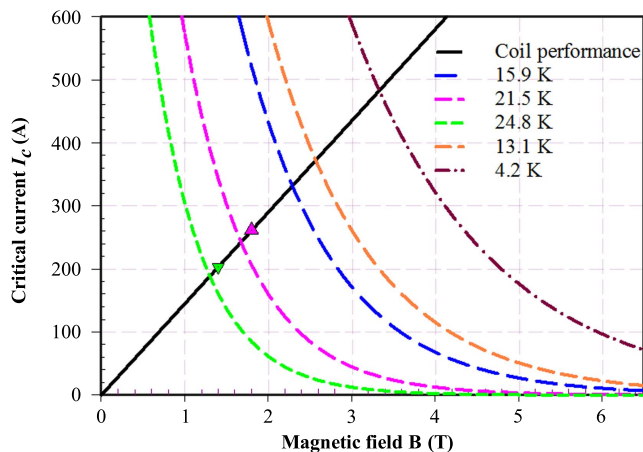


Figure 8. Critical current, I_c , versus B for the conductor at different temperatures is shown as a set of dashed lines. The load line of the magnet, calculated using FEM is also shown. Here the load line represents the highest field in the winding, which occurs in the plane of the coil, and at the smallest radius of the winding. Triangles show the near intersection of the load line and short sample response.

field, and this will determine I_c . The engineering critical current density (of the magnet winding) used in this modelling was $J_e = 1.60 \times 10^8 \text{ A m}^{-2}$; this is consistent with a current in the wire of 280 A.

3.4. Performance of the coil segment

We used the results of figure 7 to construct a load line for the coil (representing the highest field in the winding, at the inner boundary of the coil within the midplane). We then generated I_c versus B curves for the conductor from fitting equation (6) to 4.2 K measurements of a short sample of the conductor (1 m length, wound onto an ITER barrel). These curves are displayed for different temperatures in figure 8 along with the coil load line. We see that the load line reached the short sample limit at 21.5 K and above. In fact, the coil load line is 104% of short sample at 21.5 K and 120% of short sample at 24.8 K, this error is due to uncertainty in I_c of the conductor extrapolated to higher temperatures, but nevertheless indicates a high level of agreement between coil and conductor. The coil I_c at 15.9 K and 1.93 T is 280 A, which is below the short sample limit, but still above the operational design current of the coil, and thus represents a success.

3.5. System integration (joints, persistent switch, and quench protection)

The coil developed and tested in this paper is just one part of an overall MRI magnet system. Considering for a moment the background magnet portion of the system only, we still need to demonstrate the full complement of six main coils and two shielding coils, as well as superconducting joints, persistent switches, the mechanical structure and cryostat. A significant amount of progress has been made in this area by our collaboration (Hyper Tech, OSU, and Case-Western), including the demonstration of a working persistent joint, and designs for persistent switches, the mechanical and thermal structure, and a

quench protection scheme [22]. In this work a W&R style type joint (based on HTR strand 3700) was tested inductively using a decay method. The lowest resistance of the joint was measured to be $R = 4 \times 10^{-12} \Omega$. We are presently working to lower this resistance further and to further increase joint capacity (240 A at 2 T, 4 K). The present persistent switch design uses a bifilar winding of MgB_2 co-wound with a resistive wire around a Cu bobbin. Simulations have shown the acceptable performance can be achieved with this design, requiring between 200–800 m of wire [22]. For quench protection, we have assumed an active quench protection approach, with a heaters driven by the discharge of a capacitor, as described in [22]. While NbTi based MRI systems use passive protection, the much larger minimum quench energy and much slower normal zone propagation velocity argue for an active scheme for MgB_2 MRI systems. While the full development of all of these components are needed for a full MRI magnet demonstration, this paper has focused on the demonstration of an individual coil, made in a R&W mode, and cooled via conduction.

4. Conclusions

A R&W MgB_2 coil segment prototype has been fabricated and tested. The coil was developed as part of a development effort for a conduction-cooled, MgB_2 -based, whole-body image guided radiation therapy MRI. The coil was 0.9 m OD and required 1.7 km of 18 filament, MRI-style conductor. The coil was instrumented with temperature sensors, strain sensors, and voltage taps, and I_c was measured as a function of temperature. The coil exceeded its operational target of $I = 200 \text{ A}$ at 13.1 K and 0.75 T, and the load line reached the short sample limit at 21.5 K and above. These measurements demonstrate the viability of conduction-cooled MgB_2 background coils as a replacement for expensive LHe cooled NbTi background coils in future MRI devices.

Acknowledgments

This work was supported by the National Institute of Biomedical Imaging and Bioengineering, under grant R01EB018363, and under an NIH bridge grant program grant 5R44CA144415-06.

ORCID iDs

D Zhang <https://orcid.org/0000-0003-3332-8849>

C Kovacs <https://orcid.org/0000-0002-3625-7516>

M Majoros <https://orcid.org/0000-0001-8167-2287>

References

- [1] Wang Z, Van Oort J M and Zou M X 2012 Development of superconducting magnet for high-field MR systems in China *Physica C* **482** 80–6
- [2] Stenvall A, Hiltunen I, Korpela A, Lehtonen J, Mikkonen R, Viljamaa J and Grasso G 2007 A checklist for designers of cryogen-free MgB_2 coils *Supercond. Sci. Technol.* **20** 386

- [3] Laskaris E T, Ackermann R, Dorri B, Gross D, Herd K and Minas C 1995 A cryogen-free open superconducting magnet for interventional MRI applications *IEEE Trans. Appl. Supercond.* **5** 163
- [4] Wilson M N 1983 *Superconducting Magnets* (Oxford: Clarendon)
- [5] Parizh M, Lvovsky Y and Sumption M 2016 Conductors for commercial MRI magnets beyond NbTi: requirements and challenges *Supercond. Sci. Technol.* **30** 014007
- [6] Li G Z, Sumption M D, Susner M A, Yang Y, Reddy K M, Rindfleisch M A, Tomsic M J, Thong C J and Collings E W 2012 The critical current density of advanced internal-Mg-diffusion-processed MgB₂ wires *Supercond. Sci. Technol.* **11** 115023
- [7] Susner M A, Yang Y, Sumption M D, Collings E W, Rindfleisch M A, Tomsic M J and Marzik J V 2011 Enhanced critical fields and superconducting properties of pre-doped B powder-type MgB₂ strands *Supercond. Sci. Technol.* **24** 012001
- [8] Braccini V, Nardelli D, Penco R and Grasso G 2007 Development of *ex situ* processed MgB₂ wires and their applications to magnets *Physica C* **456** 209–17
- [9] Tomsic M, Rindfleisch M, Yue J, McFadden K, Doll D, Phillips J, Sumption M D, Bhatia M, Bohnenstiehl S and Collings E W 2007 Development of magnesium diboride (MgB₂) wires and magnets using *in situ* strand fabrication method *Physica C* **456** 203–8
- [10] Sumption M D, Bhatia M, Rindfleisch M, Tomsic M and Collings E W 2005 Transport and magnetic J_c of MgB₂ strands and small helical coils *Appl. Phys. Lett.* **86** 102501
- [11] Sumption M D, Bhatia M, Buta F, Bohnenstiehl S, Tomsic M, Rindfleisch M, Yue J, Phillips J, Kawabata S and Collings E W 2005 Solenoidal coils made from monofilamentary and multifilamentary MgB₂ strands *Supercond. Sci. Technol.* **18** 961
- [12] Sumption M D, Bohnenstiehl S, Buta F, Majoros M, Kawabata S, Tomsic M, Rindfleisch M, Phillips J, Yue J and Collings E W 2007 Wind and react and react and wind MgB₂ solenoid, racetrack and pancake coils *IEEE Trans. Appl. Supercond.* **17** 2286–90
- [13] Sumption M D, Bhatia M, Buta F, Bohnenstiehl S, Tomsic M, Rindfleisch M, Yue J, Phillips J, Kawabata S and Collings E W 2007 Multifilamentary MgB₂-based solenoidal and racetrack coils *Physica C* **458** 12–20
- [14] Takahashi M, Tanaka K, Okada M, Kitaguchi H and Kumakura H 2005 Relaxation of a trapped magnetic field in a 100 m long class MgB₂ solenoid coil in persistent current mode operation *Supercond. Sci. Technol.* **18** 373
- [15] Park D K, Hahn S, Bascuñán J and Iwasa Y 2011 Active protection of an MgB₂ test coil *IEEE Trans. Appl. Supercond.* **21** 2402–5
- [16] Ye L, Cruciani D, Xu M, Mine S, Amm K and Schwartz J 2015 Magnetic field dependent stability and quench behavior and degradation limits in conduction-cooled MgB₂ wires and coils *Supercond. Sci. Technol.* **28** 035015
- [17] Wang D, Ma Y, Yao C, Xu D, Zhang X and Awaji S 2017 Transport properties of multifilament MgB₂ long wires and coils prepared by an internal Mg diffusion process *Supercond. Sci. Technol.* **30** 064003
- [18] Patel D *et al* 2016 Evaluation of persistent-mode operation in a superconducting MgB₂ coil in solid nitrogen *Supercond. Sci. Technol.* **29** 04LT02
- [19] Razeti M, Angius S, Bertora L, Damiani D, Marabotto R, Modica M, Nardelli D, Perrella M and Tassisto M 2008 Construction and operation of cryogen free MgB₂ magnets for open MRI systems *IEEE Trans. Appl. Supercond.* **18** 882–6
- [20] Kim H S, Kovacs C, Rindfleisch M, Yue J, Doll D, Tomsic M, Sumption M D and Collings E W 2016 Demonstration of a conduction cooled react and wind MgB₂ coil segment for MRI applications *IEEE Trans. Appl. Supercond.* **26** 4400305
- [21] O'Brien D J, Schupp N, Pencea S, Dolan J and Sawakuchi G O 2017 Dosimetry in the presence of strong magnetic fields *J. Phys.: Conf. Ser.* **847** 012055
- [22] Baig T *et al* 2017 Conceptual designs of conduction cooled MgB₂ magnets for 1.5 and 3.0 T full body MRI systems *Supercond. Sci. Technol.* **30** 043002
- [23] Susner M A, Sumption M D, Rindfleisch M A and Collings E W 2013 Critical current densities of doped MgB₂ strands in low and high applied field ranges: the $J_c(B)$ crossover effect *Physica C* **390** 20–5
- [24] Nagamatsu J, Nakagawa N, Muranaka T, Zenitani Y and Akimitsu J 2001 Discovery of superconductivity MgB₂ with $T_c = 39$ K *Nature* **410** 63–4
- [25] Weissler G L and Robert W C 1980 *Vacuum Physics and Technology* (New York: Academic)
- [26] Matula R A 1979 Electrical resistivity of copper, gold, palladium, and silver *J. Phys. Chem. Ref. Data* **8** 1147–298
- [27] Soni A and Okram G S 2008 Resistivity and thermopower measurement setups in the temperature range of 5–325 K *Rev. Sci. Instrum.* **12** 125103
- [28] Soltanian S, Wang X L, Horvat J, Dou S X, Sumption M D, Bhatia M, Collings E W, Munroe P and Tomsic M 2005 High transport critical current density and large H_{c2} and H_{irr} in nanoscale SiC doped MgB₂ wires sintered at low temperature *Supercond. Sci. Technol.* **18** 658
- [29] Jackson D 1999 *Classical Electrodynamics* 3rd edn (New York: Wiley)
- [30] Li G Z, Yang Y, Susner M A, Sumption M D and Collings E W 2011 Critical current densities and n-values of MgB₂ strands over a wide range of temperatures and fields *Supercond. Sci. Technol.* **25** 025001